

# Nitrogen broadening of SF<sub>6</sub> transitions in the $\nu_3$ band<sup>☆</sup>

R.R. Gamache<sup>a,\*</sup>, Nelly Lacome<sup>b</sup>, Gerard Pierre<sup>c</sup>, Tony Gabard<sup>c</sup>

<sup>a</sup>Department of Environmental, Earth, and Atmospheric Sciences, The University of Massachusetts Lowell, 1 University Avenue, Lowell, MA 01854, USA

<sup>b</sup>LADIR/Spectrochimie Moléculaire, Université Pierre et Marie Curie, Bâtiment F74, 4, Place Jussieu, 75252 Paris Cedex 05, France

<sup>c</sup>Laboratoire de Physique de l'Université de Bourgogne, Faculté des Sciences Mirande, 9 Allée Alain Savary, BP 47870, 21078 Dijon Cedex, France

Received 14 August 2000; accepted 20 October 2000

## Abstract

Nitrogen induced pressure-broadened halfwidths of a number of  $\nu_3$  transitions of SF<sub>6</sub> are calculated using the complex Robert–Bonamy (CRB) formalism. The calculations are made at 200, 250, 296 and 350 K and the temperature dependence of the halfwidths are determined. The intermolecular potential is taken as a sum of the leading electrostatic and Lennard-Jones [6–12] atom–atom components. The dynamics of the collision process are correct to second order in time. The calculated halfwidths are used to simulate the  $\nu_3$  spectrum, which is compared to a simulation made using the HITRAN96 halfwidths and measurements made at the Université Pierre et Marie Curie. It is shown that simulations made using the halfwidths calculated in this work are in better agreement with the measurements. © 2001 Elsevier Science B.V. All rights reserved.

**Keywords:** Sulfur hexafluoride; Halfwidths; Line broadening; Temperature dependence of the halfwidth

## 1. Introduction

Sulfur hexafluoride, a gas of anthropogenic origin, has a number of uses as an electrical insulating gas. SF<sub>6</sub> is chemically highly stable and has the ability to impede electric breakdown [1]. It is employed in a number of high-voltage electrical and electronic equipment such as circuit breakers, transformers, and microwave components. The  $\nu_3$  band of SF<sub>6</sub> at 10.6 micron strongly absorbs CO<sub>2</sub> laser radiation, which has led to a variety of non-linear optical phenomena including saturation, pulse echoes self-induced transparency,

mode locking, passive Q-switching, optical mutation, and ir–ir double resonances [2–4]. Because of its chemical stability and diffusion properties, it is the ‘air’ in ‘Nike air’ shoes.

Sulfur hexafluoride absorbs strongly in the infrared region and hence is a strong greenhouse gas. One molecule of sulfur hexafluoride has the same global warming potential as 23,900 molecules of carbon dioxide [5]. It can be detected in situ at very low concentrations [6] and hence has been used as a meteorological tracer [7,8]. SF<sub>6</sub> was one of the first trace species detected in the stratosphere via gas chromatographic separation with electron capture detectors. [9,10] As pointed out by Singh et al. [11] the atmospheric lifetime of SF<sub>6</sub> may be very long because there are no known sinks in the troposphere and SF<sub>6</sub> is transparent to UV photolysis in the stratosphere. The two mechanisms for its destruction probably occur above 50 km altitude by electron

<sup>☆</sup> This paper is dedicated to Professor Alfred Bauder in appreciation of his significant contributions to the field of microwave spectroscopy.

\* Corresponding author.

E-mail address: robert\_gamache@uml.edu (R.R. Gamache).

capture [11–13] and photolysis by energetic UV photons in the ionosphere [13]. From these studies, Ramanathan et al. [13] estimated the average atmospheric residence time of SF<sub>6</sub> to be 500 years.

Rinsland et al. [14] report the detection of sulfur hexafluoride in the lower stratosphere and upper troposphere by remote sensing measurements. They identified the  $\nu_3$  band *Q* branch at 947.9 cm<sup>-1</sup> in high resolution solar occultation spectra recorded by the ATMOS instrument [15,16] during its first flight onboard the space shuttle as part of the Space lab 3 mission.

The quantum mechanical structure of SF<sub>6</sub> is such that even with current high-resolution instruments it is impossible to resolve individual lines. Thus at the pressures studied the measured spectra demonstrate band structure. The  $\nu_3$  band region of SF<sub>6</sub> has been recorded on the Université Pierre et Marie Curie Bruker IFS120 high-resolution spectrometer. The pressure of SF<sub>6</sub> was set at 0.051 mbar and that of nitrogen to 200.7 mbar. An optical path length of 30 cm was used and the measurements were made at room temperature. Theoretical attempts to simulate this spectrum can be made if the molecular parameters are known for SF<sub>6</sub>. For the  $\nu_3$  band, the work of Pierre et al. [17] is used for the positions and intensities of the lines. The halfwidths of the lines were taken from the HITRAN database [18]. The resulting simulation does not agree with the measurement. It was found that a doubling of the HITRAN values give better agreement with the measured spectrum [19].

The halfwidths for SF<sub>6</sub> that are on the HITRAN database are from the calculations of Tejwani and Fox [20]. They employed the method of Anderson–Tsao–Curnutte (ATC) [21–24] to make the calculations. The calculations used the leading electrostatic interactions for the SF<sub>6</sub>–N<sub>2</sub> system, hexadecapole (SF<sub>6</sub>)–quadrupole (N<sub>2</sub>) and hexadecapole (SF<sub>6</sub>)–hexadecapole (N<sub>2</sub>), straight-line trajectories and the cutoff-procedure typical to the ATC method [25,26]. Tejwani and Fox made fits to halfwidth measurements for CH<sub>4</sub> broadened by SF<sub>6</sub> to get a value of the hexadecapole moment of SF<sub>6</sub> of  $\Phi(\text{SF}_6) = 30 \times 10^{-42}$  e.s.u. cm<sup>4</sup>. The recommended value of  $\Phi$  is from Birnbaum and Sutter [27],  $\Phi(\text{SF}_6) = 5.4 \times 10^{-42}$  e.s.u. cm<sup>4</sup>. Thus, the hexadecapole moment of sulfur hexafluoride, which appears squared in the calculations, was scaled by roughly 5.5 by Tejwani and Fox to give agreement between the ATC calculations and experiment.

The need for scaling the hexadecapole moment of SF<sub>6</sub> in the ATC calculations is because the SF<sub>6</sub>–X system, with X = N<sub>2</sub>, O<sub>2</sub>, is a weakly interacting system in the Oka sense. [28] The leading electrostatic component to the intermolecular potential is hexadecapole–quadrupole. Thus the interaction is weak in terms of the electrostatic forces. The potential must be improved somehow to account for close collisions.

An improved potential for weakly interacting species was introduced in the pioneering work of Robert and Bonamy [29] for diatomic–atom and diatomic–diatomic systems. In this work an atom–atom potential (a Lennard-Jones 6–12 potential [30] between the atoms of the radiating and perturbing molecules) was added to the electrostatic components of the intermolecular potential. The atom–atom potential accounts for close intermolecular separation. The atom–atom potential was later extended by Labani et al. [31–33] to consider asymmetric rotor molecules, such as H<sub>2</sub>O and O<sub>3</sub>, in collision with diatomic and asymmetric rotor molecules. Labani et al. used the expansion of 1/*R* given by Hirschfelder et al. [34] carried out to fourth order. The atom–atom potential was extended by Neshyba and Gamache [35] to general order for XY<sub>2</sub>–AB systems using the expansion of Sack. [36] The atom–atom potential was then applied to the CH<sub>4</sub>–N<sub>2</sub> system by Neshyba et al. [37], to CH<sub>4</sub>–Ar, and CH<sub>4</sub>–He by Gabard [38,39], and to H<sub>2</sub>O–X (X = N<sub>2</sub>, O<sub>2</sub>, CO<sub>2</sub>, H<sub>2</sub>, Ar) by Gamache et al. [40–48].

For weakly interacting systems, it is found that the atom–atom component of the potential can be greater than the electrostatic component of the potential [37]. Thus for the system under consideration in this work, SF<sub>6</sub>–N<sub>2</sub>, it was decided to calculate the halfwidth using the Complex Robert–Bonamy formulation with the intermolecular potential being comprised of the leading electrostatic and atom–atom components. These halfwidths will then be used in a simulation of the  $\nu_3$  region of the spectrum to compare with the measurements made at the Université Pierre et Marie Curie.

## 2. Theory

The halfwidth,  $\gamma$ , of a ro-vibrational transition  $f \leftarrow i$  are given in the complex Robert–Bonamy

(CRB) formalism by minus the imaginary part of the diagonal elements of the complex relaxation matrix. In computational form, the halfwidth is usually expressed in terms of the Liouville scattering matrix [49,50]:

$$\gamma_{f \leftarrow i} = \frac{n_2 \bar{v}}{2\pi c} \sum_{j_2} \langle J_2 | \rho_2 | J_2 \rangle \int_0^\infty 2\pi b [1 - \cos\{S_1 + \text{Im}\{S_2\}\} e^{-\text{Re}\{S_2\}}] db \quad (1)$$

where  $\bar{v}$  is the mean relative thermal velocity,  $\rho_2$  and  $n_2$  are the density operator and number density of perturbers, and  $b$  is the impact parameter.  $S_1$  and  $S_2$  are the first and second order terms in the expansion of the Liouville scattering matrix and depend on the intermolecular potential.

The Robert–Bonamy formalism was chosen for several reasons. The use of the cumulant expansion [51,52] in the formulation of the theory eliminates an awkward cutoff procedure [25,26] that characterized earlier theories. In its complex form, halfwidths and line shifts can be determined from a single calculation. A short-range atom–atom potential [36,37] can be incorporated into the theory in a natural and non-redundant fashion. Finally the intermolecular dynamics are more realistic than in earlier theories, i.e. using curved rather than straight-line trajectories. In our implementation, these trajectories are determined by the isotropic part of the atom–atom potential.

In the CRB method, the real and imaginary components of the expanded  $S$  matrix are present in the expression for the halfwidth and line shift, an effect not achieved in Anderson–Tsao–Curnutte theory [21–24]. The inclusion of these terms has been shown to give better agreement with measurement [46]. In order to use these terms certain molecular constants and parameters must be known for both the radiating and perturbing molecules including: the dipole moment and its vibrational dependence, the polarizability and its vibrational dependence, and the ionization potential. Because the polarizability and its vibrational dependence are not known for sulfur hexafluoride, the  $S_1$  term in Eq. (1) cannot be calculated. It is also found that the  $\text{Im}\{S_2\}$  term is small and will be neglected in the calculations.

The potential employed in the calculations consists

of the leading electrostatic components for the SF<sub>6</sub>–N<sub>2</sub> pair (hexadecapole moments of SF<sub>6</sub> with the quadrupole moment of N<sub>2</sub> and an atom–atom component) [35,37]. The isotropic component of the atom–atom potential is used to define the trajectory of the collision within the semiclassical model of Robert and Bonamy [29].

The atom–atom potential is defined as the sum of pair-wise Lennard-Jones 6–12 interactions [30] between atoms of the molecules ( $i \equiv \text{SF}_6$  and  $j \equiv \text{N}_2$ ),

$$V^{\text{at-at}} = \sum_{i=1}^n 4\epsilon_{i2} \left\{ \frac{\sigma_{i2}^{12}}{r_{i2}^{12}} - \frac{\sigma_{i2}^6}{r_{i2}^6} \right\} \quad (2)$$

$$V^{\text{atom-atom}} = \sum_{i,j}^{n_i, n_j} 4\epsilon_{ij} \left\{ \frac{\sigma_{ij}^{12}}{r_{ij}^{12}} - \frac{\sigma_{ij}^6}{r_{ij}^6} \right\}.$$

The subscripts  $i$  and  $j$  run over the  $n_i$  atoms of SF<sub>6</sub> and the  $n_j$  atoms of N<sub>2</sub>, and  $\epsilon_{ij}$  and  $\sigma_{ij}$  are the Lennard-Jones parameters for the atomic pairs. The heteronuclear atom–atom parameters can be constructed from homonuclear atom–atom parameters ( $\epsilon_i$  and  $\sigma_i$ ) by the ‘combination rules’ [34]

$$\epsilon_{ij} = \sqrt{\epsilon_i \epsilon_j} \quad \sigma_{ij} = \frac{\sigma_i + \sigma_j}{2}, \quad (3)$$

The atom–atom distance,  $r_{ij}$  can be expressed in terms of the center of mass separation,  $R$ , via the expansion of Sack [36]. Using this fact, Gray and Gubbins [53,54] have shown how the atom–atom potential may be expressed in the form of a spherical tensor expansion:

$$V = \sum_{\ell_1 \ell_2} \sum_{\substack{n_1 \\ \ell}} \sum_{\substack{w, qq \\ m}} \frac{U(\ell_1 \ell_2 \ell, n_1 w q)}{R^{q+\ell_1+\ell_2+2w}} \otimes C(\ell_1 \ell_2 \ell, m_1 m_2 m) D_{m_1 n_1}^{\ell_1}(\Omega_1) D_{m_2 0}^{\ell_2}(\Omega_2) Y_{\ell m}(\omega) \quad (4)$$

where  $C(\ell_1 \ell_2 \ell; m_1 m_2 m)$  is a Clebsch–Gordan coefficient,  $\Omega_1 = (\alpha_1, \beta_1, \gamma_1)$  and  $\Omega_2 = (\alpha_2, \beta_2, \gamma_2)$  are the Euler angles describing the molecular fixed axis relative to the space fixed axis. Subscripts 1 and 2 refer to the active molecule (SF<sub>6</sub>) and its collision partner (N<sub>2</sub>), respectively, and  $\omega = (\theta, \phi)$  describes the orientation of the vector joining the centers of

Table 1  
Molecular constants used in the RB calculations

| System          | Parameter  |                    |
|-----------------|--|--------------------|
|                 | Electrostatic moment                                     |                    |
| SF <sub>6</sub> | $\Phi = 5.4 \times 10^{-42}$ esu cm <sup>4</sup>         |                    |
| N <sub>2</sub>  | $\theta_{zz} = -1.4 \times 10^{-26}$ esu cm <sup>2</sup> |                    |
|                 | Atom–atom parameters                                     |                    |
|                 | $\sigma$ (Å)   | $\epsilon/k_B$ (K) |
| S–N             | 3.495  | 76.7               |
| F–N             | 2.995  | 45.2               |

mass of the molecules with respect to space fixed axis.  $R$  is the center of mass separation. The powers  $w$  and  $q$  (integers) depend upon the interaction assumed, and the coefficients  $U(\dots)$  are given in Refs. [41,53].

The atom–atom potential is in a form of a spherical tensor expansion in  $1/R$  ( $R$  = intermolecular separation). Since the expansion in  $(1/R)$  must be truncated, we also devote some discussion to questions of the convergence of calculated data. The order of the expansion has been discussed by Labani et al. [31] and by Gamache et al. [35,37,44].

The second-order term is the complex analog of that appearing in the familiar ATC theory [21–24]:

$$S_2 = S_{2,i_2}^* + S_{2,f_2} + S_{2,middle} \quad (5)$$

where the notation is that of Anderson [21]. The case in which the imaginary part of  $S_2$  is ignored has been discussed in the literature [21–24,55,56]. The *outer* terms are complex functions and can be written in the form:

$$S_{2,f_2} = \frac{1}{\hbar^2 [J_f][J_2]} \sum_{\ell_1 \ell_2} \sum_{n^a n^b} D(\ell_1 \ell_2, \mathbf{n}^a \mathbf{n}^b, J_f J_{f'}, J_2 J_{2'}) \times F_{n^a n^b}^{\ell_1 \ell_2}(\omega_{f_2 f_2'}) \quad (6)$$

where  $[J] = 2J + 1$ ,  $\mathbf{n} = (n_1, n_2)$  and  $\omega_{f_2 f_2'} = (E_{f'} - E_f + E_{2'} - E_2)$ , the  $E$ 's being the energies of the states  $f'$ ,  $f$ ,  $2'$  and  $2$ , respectively.  $S_{2,i_2}$  is obtained from Eq. (6) by replacing  $f$  with  $i$ . The  $D$  terms are reduced matrix elements for the internal states of the radiator and perturber [37] and the  $F$  terms are the

resonance functions, for the real and imaginary terms, [41] for the potential discussed above.

### 3. Calculations

The transitions studied in the present work correspond to the most up-to-date data for the  $\nu_3$  band of SF<sub>6</sub> [17]. This data consist of 11 495 transitions. The states are labeled by the rotational quantum number,  $J$ , the symmetry ( $A_1, A_2, E, F_1$ , or  $F_2$ ), and the alpha,  $\alpha$ , indices, which are order indices that appear when diagonalizing a Hamiltonian block at fixed  $J$  and symmetry in the list of degenerate states. All transitions that have intensity greater than  $0.1 \text{ cm}^{-2} \text{ atm}^{-1}$  and  $J'' \leq 44$  were selected from these transitions. This selection results in 2477 transitions from the original list.

All molecular parameters used in this work are the best available values from the literature. No molecular constants are adjusted to give better agreement with experiment. The hexadecapole moment of SF<sub>6</sub> was set to the value recommended by Birnbaum and Sutter [27]. The quadrupole moment of nitrogen is from Mulder et al. [57]. The heteronuclear atom–atom coefficients are from the combination rules Eq. (3) using the homonuclear atom–atom coefficients from Gray and Gubbins [53] for S and F, and from Bouanich [58] for N. The numerical values are given in Table 1.

The dynamics of the collision are determined using the parabolic approximation of Robert and Bonamy [29]. In this scheme, the isotropic part of the interaction potential is taken into account to determine the distance, effective velocity, and force at closest approach. To simplify the trajectory calculations the isotropic part of the atom–atom expansion is fit to an isotropic Lennard-Jones 6–12 potential,

$$V_{\text{iso}} = 4\epsilon \left[ \left( \frac{\sigma}{R} \right)^{12} - \left( \frac{\sigma}{R} \right)^6 \right] \quad (7)$$

giving  $\epsilon/k_B = 96.6 \text{ K}$  and  $\sigma = 3.62 \text{ \AA}$  for the SF<sub>6</sub>–N<sub>2</sub> collision pair.

To evaluate the reduced matrix elements ro-vibrational wave functions are needed. The Hamiltonian model for the ground state of SF<sub>6</sub> was developed through sixth order, such that operators up to the  $J^8$

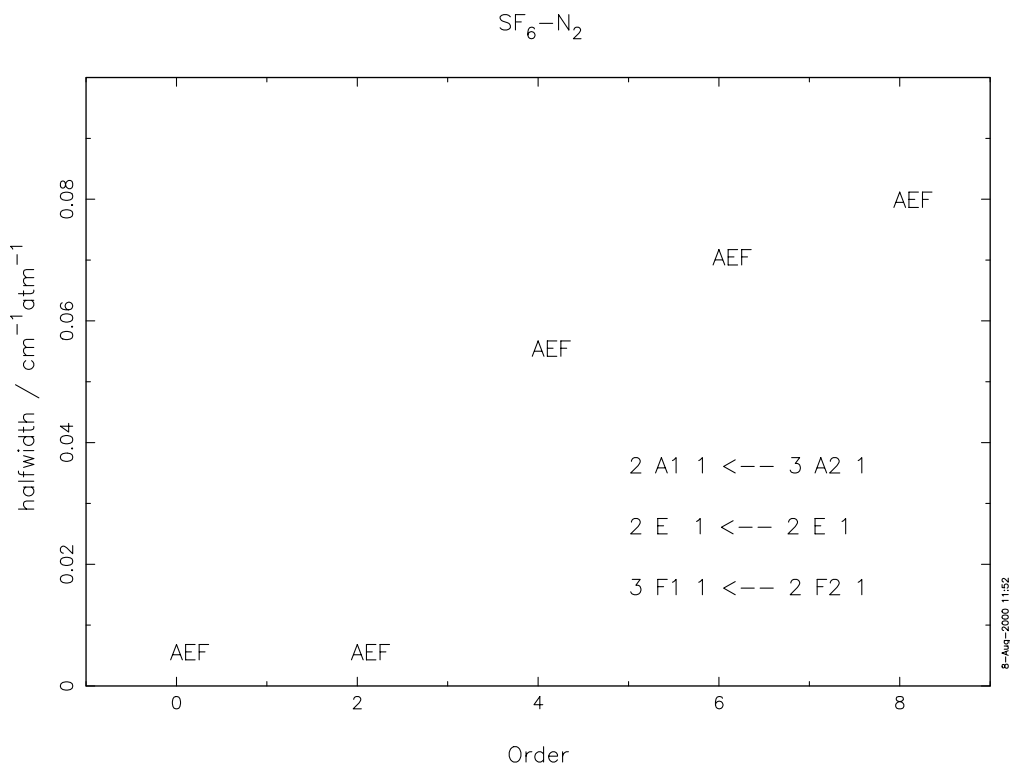


Fig. 1.  $\text{N}_2$ -broadened halfwidth in  $\text{cm}^{-1}\text{atm}^{-1}$  for three  $\nu_3$  transitions of  $\text{SF}_6$  versus the order of the atom–atom potential.

type ones, in the Amat–Nielsen ordering scheme [59], are included. For the  $\nu_3$  state, the order of development was limited to seven (i.e. all the possible operators up to the  $J^7 q_3^2$  type ones). The  $\nu_3$  state was treated as isolated from the other vibrational states. Owing to that treatment, the eigenvalues and the eigenvectors of the  $\text{SF}_6$  molecule in the ground and the  $\nu_3$  states could be evaluated using the so-called tetrahedral formalism [60]. For that purpose, we simply needed to properly correlate the symmetry labels in the  $O_h$  point group to those in the  $T_d$  point group, accounting for the parity labels ( $g$  or  $u$ ). In the ground state of  $\text{SF}_6$ , no changes were needed since the pure rotational wavefunctions are conventionally taken of  $g$  parity. But, in the  $\nu_3$  state, since the vibrational angular momentum is of  $F_{1u}$  symmetry (in the  $O_h$  group), the symmetries of the wavefunctions in  $O_h$  correlate with symmetries in  $T_d$  where the 1 and 2 subscripts are interverted. That is,  $A_{1u}$  states in  $O_h$  correlates with  $A_2$  symmetries in  $T_d$ ,  $A_{2u}$  with  $A_1$ ; the same is

true for  $F$  type labels and  $E$  labels do not need to be changed. With this method, the eigenvalues and eigenfunctions of  $\text{SF}_6$  were calculated in the two vibrational states of interest up to  $J = 50$  using the most up-to-date molecular parameters [17]. The associated molecular Hamiltonian reproduces the experimental line positions with very high accuracy. The RMS for the 321 observed data in saturated absorption up to  $J \approx 100$  is less than 1 MHz for this order of development in  $\nu_3$  and can decrease down to 40 kHz at the 10th order of development.

Starting from the above results, expressed in the cubic (or equivalently, tetrahedral, as explained) formalism, the wavefunctions were subsequently expressed in classical, or spherical, basis following a procedure similar to that described in Ref. [36]. The only slight difference is that we have to specify the parity label since we are concerned with the  $0(3) \supset O_h$  chain of groups. More precisely, a given eigenfunction is expressed as a linear combination of

basis functions through a unitary transformation  $U$ :

$$|J_g C_\tau \alpha \sigma\rangle = \sum_{N, C_{rg}, \{v_s\}, C_{v\tau}} U_{N, C_{rg}, \{v_s\}, C_{v\tau}}^{J_g, C_\tau, \alpha} \times |J_g N C_{rg}; \{v_g\} C_{v\tau}; C_\tau \sigma\rangle \quad (8)$$

where  $J$  is the total angular momentum,  $C$  is the symmetry of the wavefunction and  $\tau$  is the parity label. Since the eigenfunctions are obtained by numerical diagonalization, they are numbered by an index  $\alpha$  in increasing energy order at fixed  $J$ , symmetry  $C$  and polyad. In addition, for  $E$  and  $F$  type states, the eigenvalues are degenerated with respect to the component  $\sigma$  of the symmetry (1 or 2 for the  $E$  symmetry and  $x$ ,  $y$ , or  $z$  for the  $F$  type symmetries). The basis functions in the right hand side of the above equation are obtained by coupling rotational and vibrational basis functions to form a function of final symmetry  $C_\tau$  in  $O_h$ . Here,  $C_{rg}$  is the rotational symmetry and  $N$  is the multiplicity index of that symmetry when decomposing the  $J_g$  irreducible representation of  $O(3)$  as a direct sum of representations of  $O_h$ .  $\{v_s\}$  is a set of vibrational quantum numbers which identifies a given vibrational basis function inside a given polyad and  $C_{v\tau}$  is the associated symmetry.

In the ground state of SF<sub>6</sub>, only the rotational labels are relevant and a given wavefunction can be expressed in the classical  $J, K$  basis through the  $\mathbf{G}$  unitary transformation [61]

$$|J_g C_g \alpha \sigma\rangle = \sum_N U_N^{J_g, C_g, \alpha} |J_g N; C_g \sigma\rangle = \sum_{N, K} U_N^{J_g, C_g, \alpha} \times (J_g) G_{N C_g \sigma}^K |J_g K\rangle \quad (9)$$

In the  $\nu_3$  state, treated as isolated, the only vibrational labels that need to be introduced are those of the vibrational angular momentum, equal to one, of symmetry  $1_u$  in  $O(3)$  and of symmetry  $F_{1u}$  in  $O_h$ . When expressing wavefunctions in a classical basis, we need first to transform the basis function from an  $O_h$  coupling scheme to an  $O(3)$  coupling scheme. This is done by a unitary transformation using the  $K$  isoscalar factors for the considered chain of groups [60], and allows the extraction of the  $R_u$  pure rotational quantum number. The associated  $K_R$  projection quantum numbers are obtained using a  $\mathbf{G}$  transforma-

tion as above, i.e.

$$|J_g C_u \alpha \sigma\rangle = \sum_{N, C_{rg}} U_{N, C_{rg}, \{3\}, F_{1u}}^{J_g, C_u, \alpha} |J_g N C_{rg}; \{3\} F_{1u}; C_u \sigma\rangle = \sum_{N, C_{rg}, R_u, N_R} U_{N, C_{rg}, \{3\}, F_{1u}}^{J_g, C_u, \alpha} (-1)^R \times \left(\frac{2R+1}{3}\right)^{1/2} K_{(N C_{rg} 0 F_{1u} N_R C_u)}^{(J_g 1_u R_u)} \times |(J_g 1_u) R_u N_R C_u \sigma\rangle = \sum_{N, C_{rg}, R_u, N_R, K_R} U_{N, C_{rg}, \{3\}, F_{1u}}^{J_g, C_u, \alpha} (-1)^R \times \left(\frac{2R+1}{3}\right)^{1/2} K_{(N C_{rg} 0 F_{1u} N_R C_u)}^{(J_g 1_u R_u)} \times (R_u) G_{N_R C_u \sigma}^{K_R} |(J_g 1_u) R_u K_R\rangle \quad (10)$$

where  $N_R$  is a multiplicity index similar to the  $N$  index.

Expressed in such basis, the wavefunctions of the two vibrational states may be used to calculate the matrix elements of the intermolecular potential using relations like Eqs. (15) and (16) of Ref. [36]. But, we need to emphasize an important point here. All the angular operators, related to SF<sub>6</sub>, which appear in the intermolecular potential are given by linear combinations of WIGNER matrices with given projection quantum numbers. Such combinations have already been given in the case of methane [38]. For SF<sub>6</sub>, only the even-rank combinations are possible, due to symmetry. This means that the corresponding operators are of  $A_{1g}$  symmetry in  $O_h$ . As stated by the WIGNER–ECKART theorem, the matrix element of any operator, in this group, is proportional to a  $F$  coupling symbol [60]:

$$\langle \{\gamma\} C_\tau \sigma | T^{(A_{1g})} | \{\gamma'\} C'_\tau \sigma' \rangle \propto F \begin{pmatrix} C_\tau & A_{1g} & C'_\tau \\ \sigma & & \sigma' \end{pmatrix} \quad (11)$$

where  $\{\gamma\}$  and  $\{\gamma'\}$  are possible supplementary

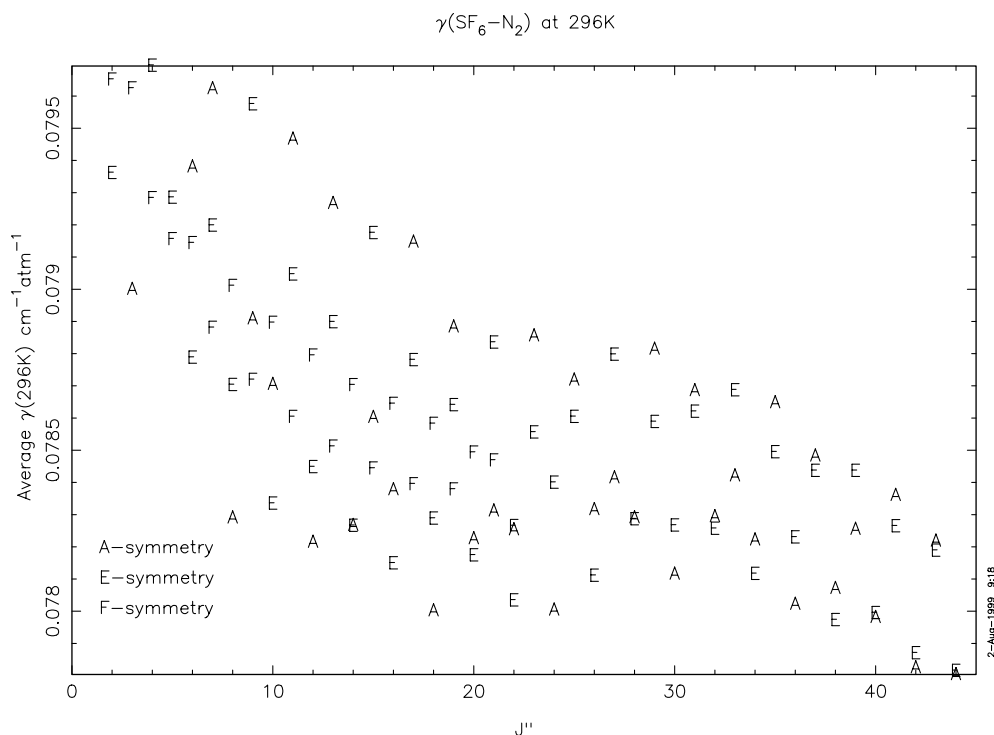


Fig. 2. Average  $\text{N}_2$ -broadened halfwidths in units of  $\text{cm}^{-1} \text{atm}^{-1}$  versus the rotational quantum number  $J''$ , plot symbols are the transition symmetry labels, A, E, and F.

labels of the basis functions. And, since

$$F \begin{pmatrix} C_\tau & A_{1g} & C'_{\tau'} \\ \sigma & & \sigma' \end{pmatrix} = \frac{1}{[C]} \delta_{C,C'} \delta_{\tau,\tau'} \delta_{\sigma,\sigma'} \quad (12)$$

$[C]$  being the dimension of the  $C$  symmetry, only matrix elements with the same symmetry, the same parity, and the same component are non zero. Thus, when working in a classical basis, it may happen that for a given WIGNER matrix with a fixed projection quantum number, some matrix elements are non-zero between wavefunctions having different symmetries and/or components in the  $O_h$  group. The discussion above allows to say that it is not useful to calculate such matrix elements since their sum over the relevant projection numbers of the angular operator of the intermolecular potential must vanish. This considerably reduces the amount of matrix elements that need to be calculated, which is fortunate for a heavy molecule like  $\text{SF}_6$  (i.e. having high  $J$  rotational states populated at the temperature of interest). In fact, this

important simplification is a well-known result, which has already been exploited in the case of methane [39,62].

The molecular constants for the states of  $\text{N}_2$  are from Huber and Herzberg [63].

Before calculations were made for the transitions discussed above, the relative importance and the order of the atom–atom potential were investigated. The order,  $\text{Order} = \ell_1 + \ell_2 + 2w$ , is defined by four integers: the maximum value of the order of development in powers of  $1/R$ ,  $\ell_{\max}$ , the maximum value of  $\ell_1 + \ell_2$ ,  $\ell_{1\max}$  and  $\ell_{2\max}$ , the maximum values of  $\ell_1$  and  $\ell_2$ , respectively. Three transitions were selected for this study; 2 A1 1  $\leftarrow$  3 A2 1, 2 E 1  $\leftarrow$  2 E 1, and 3 F1 1  $\leftarrow$  2 F2 1. Calculations were made at 296 K with the order of the atom–atom potential set at 0000 (electrostatic), 2222, 4444, 6444, and 8644. The calculated halfwidths versus the order are shown in Fig. 1. Due to the high symmetry of this system, the atom–atom potential only has

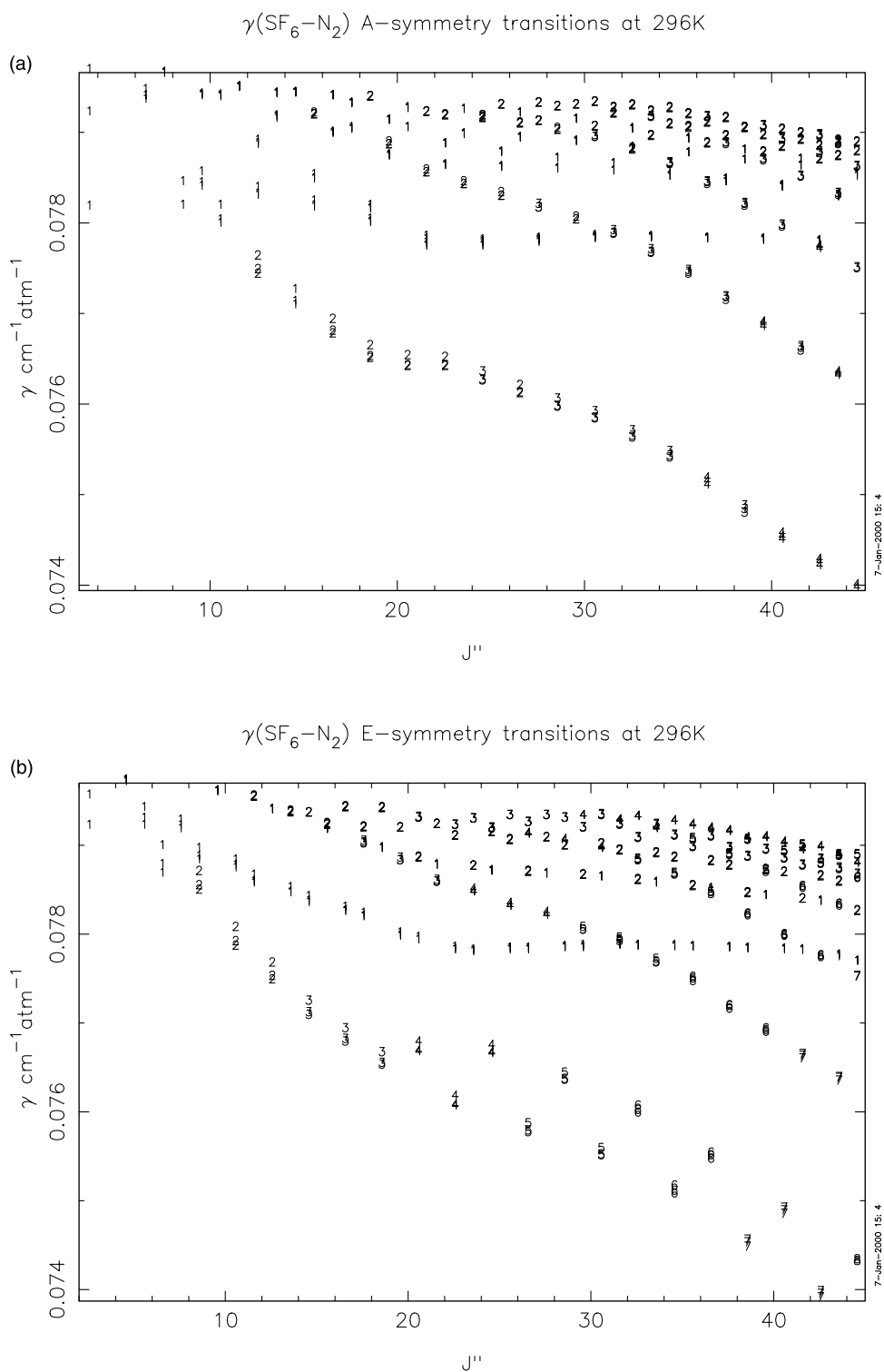


Fig. 3.  $\text{N}_2$ -broadened halfwidths in units of  $\text{cm}^{-1} \text{atm}^{-1}$  versus the rotational quantum number  $J''$ , plot symbols are the lower state label  $\alpha''$ : (a) A-symmetry transitions, (b) E-symmetry transitions, (c) F-symmetry transitions.

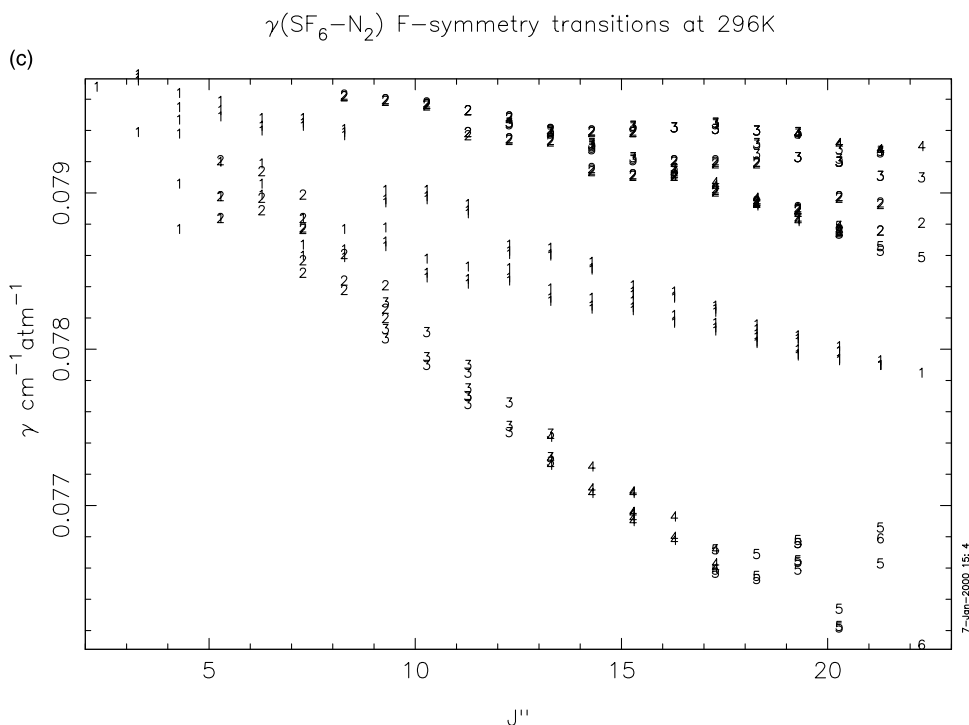


Fig. 3. (continued)

surviving terms when  $O \geq 4$ , hence the 2222 is equal to an electrostatic calculation as is evident in the figure. It is interesting to note that the atom–atom part of the potential is much more important than the electrostatic part for this system. This fact has been observed for a similar high symmetry system,  $\text{CH}_4\text{-N}_2$  [37]. The relative weakness of the electrostatic potential for this system is probably why the ATC calculations, which used only the electrostatic potential, needed to scale the hexadecapole moment of  $\text{SF}_6$  by such a large factor.

In the calculations presented here we are limited to an atom–atom expansion of 8744, which generated some 95 terms in the intermolecular potential. All further calculations employ the 8644 potential described above with only the real components of the resonance functions.

Calculations were made at 296 K for all  $A$  and  $E$  transitions and 350  $F$  transitions (up to  $\sim J'' = 22$ ) from the list of selected lines discussed above. Furthermore, in order to determine the temperature

dependence of the halfwidth, calculations were made at 200, 250, 296, and 350 K for 100  $A$ , 100  $E$ , and 50  $F$  lines. The temperature dependence of the halfwidth is the usual power law [64,65]

$$\gamma(T) = \gamma(T_0) \left[ \frac{T_0}{T} \right]^N \quad (13)$$

where the dependency is contained in the temperature exponent  $N$ .

#### 4. Results

Tables of the results of the calculations may be obtained upon request to the corresponding author (robert\_gamache@uml.edu). The calculated halfwidths at 296 K were taken and averaged as a function of the rotational quantum number for each symmetry species. These average halfwidths in units of  $\text{cm}^{-1} \text{atm}^{-1}$  are plotted in Fig. 2 versus the rotational quantum number  $J''$ . The plot symbols are the transition symmetry labels,  $A$ ,  $E$ ,

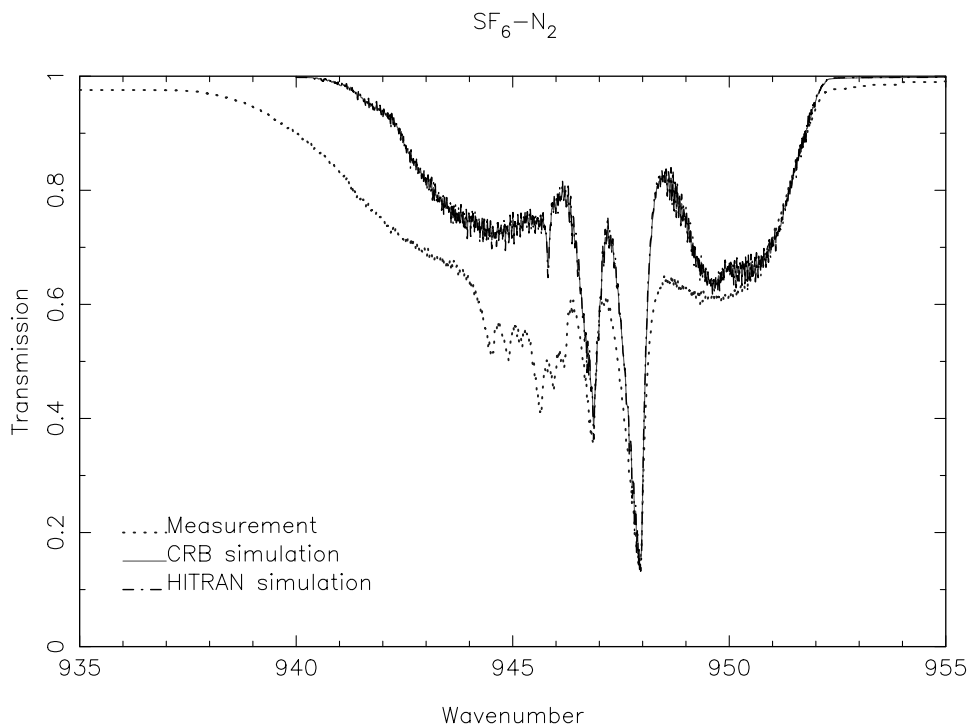


Fig. 4. Measured  $\text{SF}_6\text{-N}_2$  spectrum (dotted line) in the region from 935 to 955  $\text{cm}^{-1}$  compared with simulations using the Dijon data for the positions and intensities and the halfwidths from this work (solid line) and the halfwidths from the HITRAN database (dash-dot line).

and  $F$ . The halfwidths decrease as  $J''$  increases, however the relative magnitude of the  $A$ ,  $E$ , or  $F$  points appears to be independent of  $J''$ . The average halfwidths range from roughly 0.0778 to 0.0797  $\text{cm}^{-1} \text{atm}^{-1}$ .

In Fig. 3a, b, and c, the halfwidths at 296 K are plotted versus  $J''$  for the  $A$ -,  $E$ -, and  $F$ -symmetry transitions, respectively. The plot symbols are the lower state label  $\alpha''$  (position in the list of states). The plots show clusters of groups of three data points: these are the  $P$ -,  $Q$ -, and  $R$ -branch transitions. There does not appear to be an ordering of the halfwidth as a function of the symmetry species. The halfwidths range from roughly 0.074 to 0.0798  $\text{cm}^{-1} \text{atm}^{-1}$ .

From the calculations made at 200, 250, 296, and 350 K, the temperature dependence of the halfwidth can be determined via Eq. (13) by least-squares fitting  $\ln\{\gamma(T)/\gamma(T_0)\}$  versus  $\ln\{T_0/T\}$ . This was done for the 250 transitions considered at the four temperatures. The fit yields the slope (temperature exponent), intercept and correlation coefficient of the fit. An uncer-

tainty of the fit is determined by taking only two points at two different temperatures for a given calculation (6 combinations) and determining the corresponding slopes. The maximum difference between these 6 slopes and the one determined via the least-squares fit is taken as the uncertainty of the temperature exponent,  $\Delta N$ . The temperature exponents for the 4 point fits ranged from  $N = 1.04$  to  $N = 1.06$  with uncertainties in the range 0.11–0.14.

## 5. Experimental spectra

All spectra were recorded with a Bruker FTIR spectrometer (model IFS 120) with resolutions equal to 4 or 8.10  $\text{cm}^{-1}$ . No apodization was applied. For each spectrum an averaged of 100 scans was done. The entire optical path was maintained under vacuum. The spectrometer was equipped with a KBr/Ge beamsplitter and a photovoltaic HgCdTe liquid-nitrogen cooled detector.

$\text{SF}_6$  and  $\text{N}_2$  samples were taken from 'L'Air

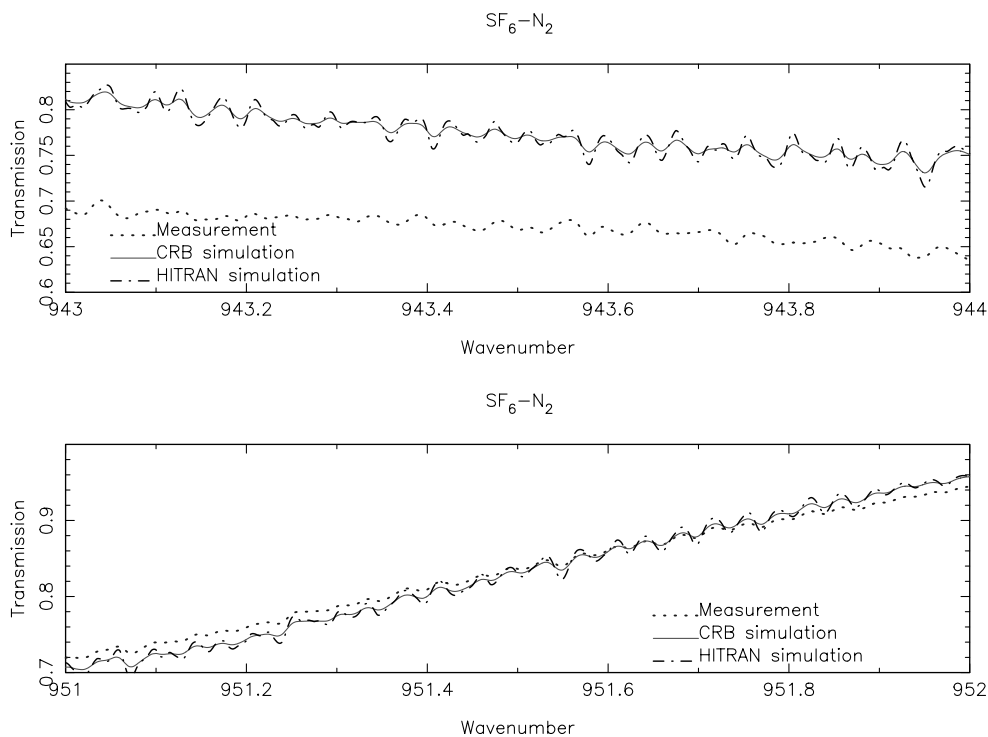


Fig. 5. Regions of the spectrum detailing the measured SF<sub>6</sub>-N<sub>2</sub> spectrum (dotted line) compared with simulations using the Dijon data for the positions and intensities and the halfwidths from this work (solid line) and the halfwidths from the HITRAN database (dash-dot line); (a) the region from 943 to 944 cm<sup>-1</sup> (b) the region from 951 to 952 cm<sup>-1</sup>.

Liquide' with a stated purity of 99.9 and 99.998%, respectively. Spectra were recorded with pressures of SF<sub>6</sub> at 0.048 mbar ( $\pm 0.001$  mbar) and pressures of N<sub>2</sub> equal to 200, 400, 600 and 1000 mbar. All samples were maintained at room temperature ( $295 \pm 1$  K) and the temperature measured with platinum sondes at several points of the cell. Reference spectra were also recorded with the N<sub>2</sub>-filled cell in order to calculate transmission spectra. For all spectra the optical path was equal to 30 cm.

## 6. Comparison of measured and simulated data

Synthetic spectra were calculated assuming additive Voigt profiles for all lines and were convoluted with a theoretical apparatus function, which takes into account the finite path difference and the finite aperture of the apparatus. A first calculation was done including the  $\nu_3$ -band para-

meters (frequencies, intensities and N<sub>2</sub>-broadened halfwidths) included in the HITRAN database. The same calculation was redone including the HITRAN frequencies and intensities along with halfwidths calculated in this work. It appeared clearly that the global calculated absorption was too weak for both cases, which was expected since the hot bands are missing in both calculations. Nevertheless, the profile in the  $\nu_3$  Q branch, especially for the 200 mbar spectrum, where the rotational structure is still slightly visible, showed a better agreement with the experimental spectrum.

In order to account for some of the hot bands in the simulations, two other calculations were done, still with additive Voigt profiles, both with the line position and intensity parameters calculated in Dijon [66] for the fundamental  $\nu_3$  and the  $\nu_3 + \nu_6 \leftarrow \nu_6$  and  $\nu_3 + 2\nu_6 \leftarrow 2\nu_6$  hot bands. The first simulation is done with the HITRAN halfwidths (dash-dot line), the second with the halfwidths

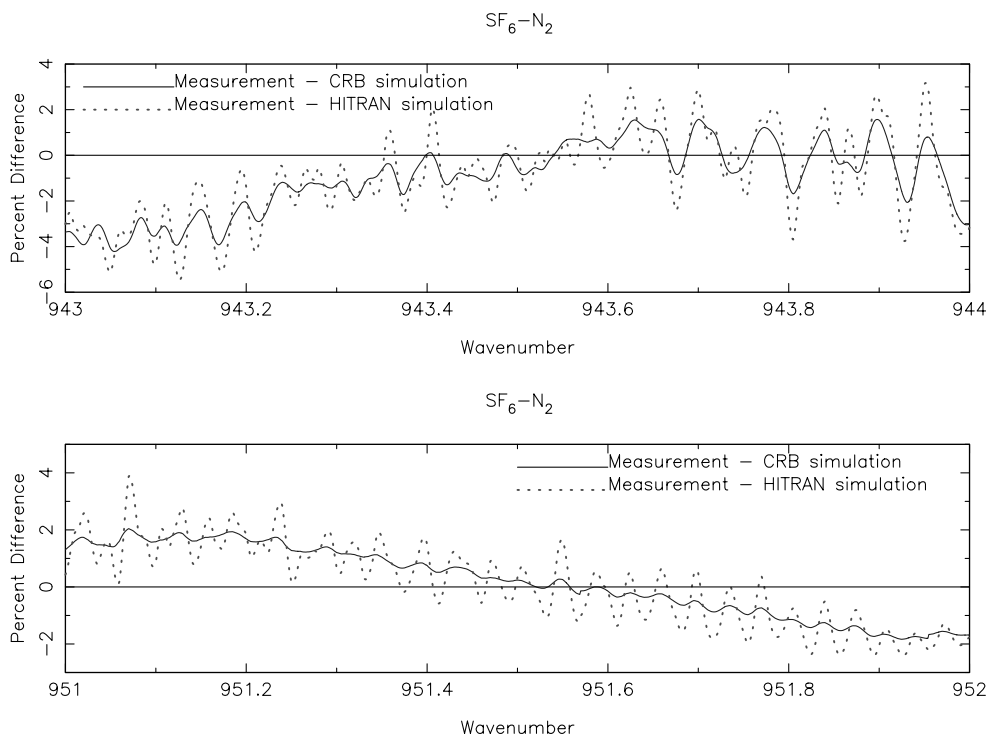


Fig. 6. Percent difference between the measured  $SF_6-N_2$  spectrum and scaled simulations using the Dijon data for the positions and intensities and the halfwidths from this work (solid line) and the halfwidths from the HITRAN database (dotted line); (a) the region from 943 to 944  $cm^{-1}$  (b) the region from 951 to 952  $cm^{-1}$ .

calculated in this work (solid line). The simulated spectra are compared with the measured one. The experimental conditions are  $P(SF_6) = 0.048(1)$  mbar,  $P(N_2) = 200.7(1)$  mbar,  $T = 295(1)$  K, an optical path of 30.0(1) cm, and resolution 0.008  $cm^{-1}$ . These data are shown in Fig. 4. From the figure it is apparent that several hot bands are still missing and therefore the calculated absorption is again too weak. It is also difficult to identify which set of halfwidths give better agreement with measurement. This determination can be done by enlarging small regions of the spectrum and looking at the detailed structure of the measurement and the simulations. Fig. 5a and b does this for the regions from 943 to 944  $cm^{-1}$  and 951 to 952  $cm^{-1}$ , respectively. In both cases, and in other regions of the spectrum that were studied, the simulations using the halfwidth values calculated here (solid line) show better agreement with the measured spectrum than does the simulation using the HITRAN halfwidths (dash-dot line).

This agreement can be better seen by scaling the simulation to agree with the measurement at one wavenumber and then calculating the percent difference (measurement-simulation). Fig. 6a and b show these results for the regions from 943 to 944  $cm^{-1}$  and 951 to 952  $cm^{-1}$ , respectively, where the simulations are scaled at 943.540  $cm^{-1}$  in Fig. 6a and at 951.558  $cm^{-1}$  in Fig. 6b. Measurement minus the scaled simulation using the CRB halfwidths is shown by the solid line and measurement minus the scaled simulation using the HITRAN halfwidths is shown by the dotted line. The improved agreement for the simulation using the halfwidths determined by the CRB formalism is clear from the figures.

For higher  $N_2$  pressure the agreement appears to be improved by the change in the halfwidths but this improvement was mainly sensitive in the *R*-branch region. The test was much more difficult in the *Q*-branch region because all rotational structure was removed by pressure broadening.

## 7. Summary

Nitrogen-broadened halfwidths of SF<sub>6</sub> transitions in the  $\nu_3$  band were calculated using Complex Robert–Bonamy theory. The calculations were made at 200, 250, 296 and 350 K and the temperature dependence of the halfwidths determined. These data were used to simulate the fundamental  $\nu_3$  and the  $\nu_3 + \nu_6 \leftarrow \nu_6$  and  $\nu_3 + 2\nu_6 \leftarrow 2\nu_6$  hot bands in the  $\nu_3$  region. The simulated spectra were compared to measurements of the spectra in the  $\nu_3$  region. The halfwidths determined by the CRB method yield simulated spectra that give better agreement with measurement than do the halfwidths currently on the HITRAN database. This is not surprising since those on the database are from scaled ATC calculations done 14 years ago.

We also note that the simulations assume additive Voigt profiles for all the lines. It is expected that some line mixing will occur for this system and this has not been taken into account in the simulations.

The simulations clearly demonstrate the need to include other hot bands into the calculation. A better test will be possible only when the spectral parameters will be available for all the hot band absorbing in the area. This part of the work is in progress.

## Acknowledgements

The authors would like to thank Programme National de Chimie Atmospherique — Institut National des Sciences de l'Univers for support of this work. One of the authors (RRG) would also like to thank the National Science Foundation for support through Grants No. ATM-9415454 and ATM-9812540. Any opinions, findings, and conclusions or recommendations expressed in this material are those of the author(s) and do not necessarily reflect the views of the National Science Foundation.

## References

[1] J.A. Brown, Sulfur hexafluoride, Kirk-Othmer Encyclopedia of Chemical Technology, 2nd ed., Wiley, New York, 1966 pp. 664–671.  
 [2] J.I. Steinfeld, I. Burak, D.G. Sutton, A.V. Nowak, J. Chem. Phys. 52 (1970) 5421.  
 [3] A.V. Nowak, J.L. Lyman, J. Quant. Spectrosc. Radiat. Transfer 15 (1975) 945.

[4] E. Yablonovitch, H.W. Galbraith, C.D. Cantrell, K. Fox, C.K. Rhodes, C.D. Cantrell, in: A. Perlmutter, L.F. Scott (Eds.), The Significance of Non-linearity in the Natural Sciences, Plenum Press, New York, 1977.  
 [5] Climate Change 1995. The Science of Climate Change — Contribution of Working Group I to the Second Assessment Report of the IPCC. Cambridge UK. Cambridge University Press. Intergovernmental Panel on Climate Change. P121, 1996.  
 [6] C.A. Clemons, A.I. Coleman, B.E. Salzman, Environ. Sci. Technol. 2 (1968) 551–556.  
 [7] A. Turk, S.M. Edmonds, H.L. Mark, G.F. Collins, Environ. Sci. Technol. 2 (1968) 44–48.  
 [8] P.J. Drivas, F.H. Shair, Atmos. Environ. 8 (1974) 1155–1163.  
 [9] P.W. Krey, R.J. Lagomarsino, M. Schonberg, Geophys. Res. Lett. 4 (1977) 271–274.  
 [10] P.W. Krey, R.J. Lagomarsino, L.E. Toonkel, J. Geophys. Res. 83 (1977) 1753–1766.  
 [11] H.B. Singh, L.J. Salas, L.A. Cavanaugh, J. Air, Pollut. Control Assoc. 27 (1977) 332–336.  
 [12] H.B. Singh, L.J. Salas, H. Shigeishi, E. Scribner, Science 203 (1979) 899–903.  
 [13] V. Ramanathan, R.J. Cicerone, H.B. Singh, J.T. Kiehl, J. Geophys. Res. 90 (1985) 5547–5566.  
 [14] C.P. Rinsland, L.R. Brown, C.B. Farmer, J. Geophys. Res. 95 (1990) 5577–5585.  
 [15] C.B. Farmer, O.F. Raper, High resolution infrared spectroscopy from space: a preliminary report on the results of the Atmospheric Trace Molecule Spectroscopy (ATMOS) experiment on Spacelab 3, Spacelab 3 Mission Review, NASA Conf. Proc. CP-2429, 42–62, May 1986. Available as NTIS 87N22103 from Natl. Tech. Inf. Serv., Springfield, Va.  
 [16] C.B. Farmer, O.F. Raper, F.G. O'Callaghan. Final report on the first flight of the ATMOS instrument during the Spacelab 3 mission. April 29 through May 6, 1985, JPL Publ. 87–32 1987. pp. 45.  
 [17] O. Acef, Ch.J. Borde, A. Clairon, G. Pierre, B. Sartakov, J. Mol. Spectrosc. 199 (2000) 188–204.  
 [18] L.S. Rothman, C.P. Rinsland, A. Goldman, S.T. Massie, D.P. Edwards, J.-M. Flaud, A. Perrin, V. Dana, J.-Y. Mandin, J. Schroeder, A. McCann, R.R. Gamache, R.B. Wattson, K. Yoshino, K.V. Chance, K.W. Jucks, L.R. Brown, V. Nemtchinov, P. Varanasi, J. Quant. Spectrosc. Radiat. Transfer 60 (1998) 665–710.  
 [19] Maxime Petiau, Université Pierre et Marie Curie, Internal report, Paris, June 1997.  
 [20] G.D.T. Tejwani, K. Fox, J. Quant. Spectrosc. Radiat. Transfer 37 (1987) 541–546.  
 [21] P.W. Anderson. Dissertation, Harvard University 1949.  
 [22] P.W. Anderson, Phys. Rev. 76 (1949) 647.  
 [23] P.W. Anderson, Phys. Rev. 80 (1950) 511.  
 [24] C.J. Tsao, B. Curnutte Jr., J. Quant. Spectrosc. Radiat. Transfer 2 (1962) 41.  
 [25] R.H. Tipping, R.M. Herman, J. Quant. Spectrosc. Radiat. Transfer 10 (1970) 881.  
 [26] R.H. Tipping, R.M. Herman, J. Quant. Spectrosc. Radiat. Transfer 10 (1970) 897.

- [27] G. Birnbaum, H. Sutter, *Mol. Phys.* 42 (1981) 21.
- [28] T. Oka, in: D.R. Bates (Ed.), *Advances in Atomic and Molecular Physics*, Academic Press, New York, 1973.
- [29] D. Robert, J. Bonamy, *J. Physiq.* 40 (1979) 923.
- [30] J.E. Lennard-Jones, *Proc. Roy. Soc. A* 106 (1924) 463.
- [31] B. Labani, J. Bonamy, D. Robert, J.M. Hartmann, J. Taine, *J. Chem. Phys.* 84 (1986) 4256.
- [32] J.M. Hartmann, J. Taine, J. Bonamy, B. Labani, D. Robert, *J. Chem. Phys.* 86 (1987) 144.
- [33] B. Labani, J. Bonamy, D. Robert, J.M. Hartmann, *J. Chem. Phys.* 87 (1987) 2781.
- [34] J.O. Hirschfelder, C.F. Curtiss, R.B. Bird, *Molecular Theory of Gases and Liquids*, Wiley, New York, 1964.
- [35] S.P. Neshyba, R.R. Gamache, *J. Quant. Spectrosc. Radiat. Transfer* 50 (1993) 443.
- [36] R.A. Sack, *J. Math. Phys.* 5 (1964) 260.
- [37] S.P. Neshyba, R. Lynch, R. Gamache, T. Gabard, J.-P. Champion, *J. Chem. Phys.* 101 (1994) 9412.
- [38] T. Gabard, J.-P. Champion, *J. Quant. Spectrosc. Radiat. Transfer* 52 (1994) 303–317.
- [39] T. Gabard, *J. Quant. Spectrosc. Radiat. Transfer* 59 (1998) 287–302.
- [40] R.R. Gamache, S. Neshyba, J.J. Plateaux, A. Barbe, L. Régalia, J.B. Pollack, *J. Mol. Spectrosc.* 170 (1995) 131.
- [41] R. Lynch, R.R. Gamache, S.P. Neshyba, *J. Chem. Phys.* 105 (1996) 5711.
- [42] R.R. Gamache, R. Lynch, L.R. Brown, *J. Quant. Spectrosc. Radiat. Transfer* 56 (1996) 471.
- [43] R.R. Gamache, R. Lynch, J.J. Plateaux, A. Barbe, *J. Quant. Spectrosc. Radiat. Transfer* 57 (1997) 485.
- [44] R. Lynch, R.R. Gamache, S.P. Neshyba, *J. Quant. Spectrosc. Radiat. Transfer* 59 (1998) 595–613.
- [45] R. Lynch, R.R. Gamache, S.P. Neshyba, *J. Quant. Spectrosc. Radiat. Transfer* 59 (1998) 615–626.
- [46] R.R. Gamache, R. Lynch, S.P. Neshyba, *J. Quant. Spectrosc. Radiat. Transfer* 59 (1998) 319–335.
- [47] A. Bauer, M. Godon, J. Carlier, R.R. Gamache, *J. Quant. Spectrosc. Radiat. Transfer* 59 (1998) 273.
- [48] A. Bauer, M. Godon, J. Carlier, R.R. Gamache, *J. Mol. Spectrosc.* 176 (1996) 45.
- [49] M. Baranger, *Phys. Rev.* 112 (1958) 855.
- [50] A. Ben-Reuven, *Spectral Line Shapes in Gases in the Binary-Collision Approximation*, in: I. Prigogine, S.A. Rice (Eds.), *Adv. Chem. Phys.*, Academic Press, New York, 1975.
- [51] R. Kubo, *J. Phys. Soc. Jpn.* 17 (1962) 1100.
- [52] C. Bloch, *Nucl. Phys.* 7 (1958) 451.
- [53] C.G. Gray, K.E. Gubbins, *Theory of Molecular Fluids*, Clarendon Press, Oxford, 1984.
- [54] C.G. Gray, *Can. J. Phys.* 46 (1968) 135.
- [55] G. Yamamoto, T. Aoki, *J. Quant. Spectrosc. Radiat. Transfer* 12 (1972) 227.
- [56] M.N. Moazzen-Ahmadi, J.A. Roberts, *J. Mol. Spectrosc.* 96 (1982) 336.
- [57] F. Mulder, G. Van Dijk, A. Van der Avoird, *Mol. Phys.* 39 (1980) 407–425.
- [58] J.-P. Bouanich, *J. Quant. Spectrosc. Radiat. Transfer* 47 (1992) 243–250.
- [59] G. Amat, H.H. Nielsen, G. Tarrago, *Rotation-vibration of Polyatomic Molecules*, Marcel Dekker, New York, 1971.
- [60] J.-P. Champion, M. Loete, G. Pierre, *Spherical top spectra*, in: K. Narahari Rao, A. Weber (Eds.), *Spectroscopy of the Earth's Atmosphere and Interstellar Medium*, Academic Press, USA, 1992, pp. 339–422.
- [61] J.-P. Champion, G. Pierre, F. Michelot, J. Moret-Bailly, *Composantes cubiques normales des tenseurs spheriques*, *Can. J. Phys.* 55 (6) (1977) 512–520.
- [62] T. Gabard, *J. Quant. Spectrosc. Radiat. Transfer* 57 (1997) 177–196.
- [63] K.P. Huber, G. Herzberg, *Molecular Spectra and Molecular Structure, Constants of Diatomic Molecules*, Van Nostrand, New York, 1979.
- [64] R.R. Gamache, *J. Mol. Spectrosc.* 114 (1985) 31–41.
- [65] R.R. Gamache, L.S. Rothman, *J. Mol. Spectrosc.* 128 (1988) 360–369.
- [66] G. Pierre, unpublished data, 2000.